

# Formation of feedforward networks and frequency synchrony by spike-timing-dependent plasticity

Naoki Masuda · Hiroshi Kori

Received: 28 August 2006 / Revised: 11 December 2006 / Accepted: 23 January 2007 / Published online: 28 March 2007  
© Springer Science + Business Media, LLC 2007

**Abstract** Spike-timing-dependent plasticity (STDP) with asymmetric learning windows is commonly found in the brain and useful for a variety of spike-based computations such as input filtering and associative memory. A natural consequence of STDP is establishment of causality in the sense that a neuron learns to fire with a lag after specific presynaptic neurons have fired. The effect of STDP on synchrony is elusive because spike synchrony implies unitary spike events of different neurons rather than a causal delayed relationship between neurons. We explore how synchrony can be facilitated by STDP in oscillator networks with a pacemaker. We show that STDP with asymmetric learning windows leads to self-organization of feedforward networks starting from the pacemaker. As a result, STDP drastically facilitates frequency synchrony. Even though differences in spike times are lessened as a result of synaptic plasticity, the finite time lag remains so that perfect spike synchrony is not realized. In contrast to traditional mechanisms of large-scale synchrony based on mutual interaction of coupled neurons, the route to synchrony discovered here is enslavement of downstream neurons by upstream ones. Facilitation of such feedforward synchrony does not occur for STDP with symmetric learning windows.

**Keywords** Spike-timing-dependent plasticity · Synchronization · Feedforward networks · Complex networks

## 1 Introduction

In many neural circuits, synaptic plasticity depends on relative timing of presynaptic and postsynaptic spikes, which is known as spike-time dependent plasticity (STDP) (Gerstner et al. 1996; Bell et al. 1997; Markram et al. 1997; Bi and Poo 1998; Zhang et al. 1998). Specifically, long-term potentiation (LTP) ensues when a presynaptic neuron fires slightly before a postsynaptic neuron (of the order of 10 ms), whereas long-term depression (LTD) is elicited in the opposite case (solid line in Fig. 1). This STDP rule promotes causal relationship between a pair of neurons in the sense that the strength of a synapse that contributes to generation of postsynaptic spikes is reinforced. Computationally, STDP is useful for synaptic competition (Kempster et al. 1999; Song et al. 2000; van Rossum et al. 2000; Song and Abbott 2001), coincidence detection (Gerstner et al. 1996), spike-based associative memory (e.g. Lengyel et al. 2005), implementation of the synfire chain (Horn et al. 2000; Levy et al. 2001), generation of reproducible spatiotemporal spike patterns (Izhikevich et al. 2004; Izhikevich 2006), selection of earlier inputs, to name a few (e.g. Gerstner and Kistler 2002).

Related to neural computation, coincident firing of multiple neurons in the oscillatory regime is found in many parts of the brain and believed to play an important role (Singer and Gray 1995; Ritz and Sejnowski 1997; Buzsáki and Draguhn 2004). One could imagine that real neural networks learn to

---

**Action Editor: Wulfram Gerstner**

N. Masuda (✉)  
Amari Research Unit, RIKEN Brain Science Institute,  
2-1 Hirosawa, Wako, Saitama 351-0198, Japan  
e-mail: masuda@mist.i.u-tokyo.ac.jp

H. Kori  
Department of Mathematics, Hokkaido University, Kita 10,  
Nishi 8, Kita-Ku, Sapporo, Hokkaido 060-0810, Japan

synchronize spikes of different neurons by STDP-related synaptic plasticity, as suggested by some modeling studies. However, contribution of STDP to spike synchrony may be limited. For example, STDP can lead to division of a neural population into clusters in each of which neurons fire in spike synchrony (Horn et al. 2000; Levy et al. 2001). This self-organizing process actually necessitates homogeneous synaptic transmission delays for different synapses and puts a strong restriction on the firing period. If there is just one cluster (all neurons firing synchronously), the firing period has to be equal to the synaptic transmission delay. Similarly, if there are two clusters, the first cluster excites a synchronous volley in the second cluster after the synaptic transmission delay. The second cluster reexcites the first cluster in a similar way. The firing period is equal to the synaptic transmission delay multiplied by the number of clusters, which seems restrictive. Alternatively, coincident firing is achieved via STDP if the amount of LTP and that of LTD that are caused by a presynaptic and postsynaptic spike pair are perfectly balanced (Karbowski and Ermentrout 2002). Evolution of coincident firing survives heterogeneity in neurons and in the amount of plasticity. However, how coincident firing is affected by the imbalance between LTP and LTD remains to be explored.

Coincident firing in recurrent neural networks may not be established through STDP. In general, synchronous firing can be induced by sufficiently strong coupling between elements (Kuramoto 1984; Pikovsky et al. 2001; Gerstner and Kistler 2002). By contrast, STDP cannot strengthen the synaptic weights between two neurons bidirectionally. An increase of the synaptic weight in one direction implies a decrease in the opposite direction, and stability requires that the net decrease and the net increase are roughly balanced (Song et al. 2000; Song and Abbott 2001). Therefore, STDP does not necessarily enhance mutual interaction. Indeed, in recurrent neural networks, STDP does not necessarily support synchronous firing (Masuda and Aihara 2004). It rather reinforces reproducible spatiotemporal spike patterns composed of causal spike pairs of different neurons (Izhikevich et al. 2004; Izhikevich 2006).

We examine possible mechanisms of STDP-induced synchrony in recurrent networks of oscillatory elements. We distinguish two types of synchrony using the terminology of coupled oscillators. One type is phase synchrony, which is equivalent to spike synchrony. When neurons are in phase synchrony, they share spike timing. The other weaker notion is frequency synchrony in which neurons possibly with different

intrinsic firing rates share a common firing rate. Frequency synchrony does not imply phase synchrony. The spike time of the postsynaptic neuron can differ from that of the presynaptic neuron. According to these definitions, the previous studies cited above, which relate STDP to synchrony, regard phase synchrony.

STDP may be more relevant to frequency synchrony. For example, STDP promotes frequency synchrony, but not phase synchrony, in a hybrid circuit of an *aplysia* abdominal neuron and an emulated neuron (Nowotny et al. 2003). Unidirectional connectivity from the emulated neuron to the *aplysia* neuron eventually forms. Numerical simulations of two coupled Hodgkin–Huxley neurons (Zhigulin et al. 2003) and of large neural networks (Zhigulin and Rabinovich 2004) also support the notion that frequency synchrony is facilitated by STDP.

In the present work, we show that the standard STDP facilitates frequency synchrony to a great extent, particularly when LTP and LTD are roughly balanced. To examine how heterogeneous neurons interact to produce possible synchronization, we analyze networks of oscillators with a pacemaker. The pacemaker has a distinct natural frequency, is not affected by other oscillators, and sets the rhythm to influence other neurons. No matter whether a pacemaker is realized by a network or a single neuron, existence of pacemaker neurons is suggested in, for example, the basal ganglia (Plenz and Kitai 1999) and respiratory networks in the pre-Bötzinger complex (Ramirez et al. 2004). Furthermore, many neurons (Hutcheon and Yarom 2000) and recurrent microcircuits (Jefferys et al. 1996) are intrinsically oscillatory (also see e.g. Singer and Gray 1995), and their rhythmic activities are resistant to perturbation. These neural networks and single neurons can also serve as pacemakers. With frozen and sufficiently strong synapses, oscillator networks with pacemakers allow frequency synchrony (Kori and Mikhailov 2004). We show that STDP considerably facilitates frequency synchrony of pacemaker systems by establishing feedforward network structure whose root is the pacemaker.

For analytical tractability, we mostly deal with networks of phase oscillators in which coupling strength evolves according to STDP. Coupled phase oscillators approximate various natural systems composed of self-sustained oscillators with weak coupling (Winfrey 1980; Kuramoto 1984; Glass and Mackey 1988), including pulse-coupled neurons (Kuramoto 1991; Hansel et al. 1993, 1995; Kori 2003). We introduce the model in Section 2 and analyze simple cases of two connected oscillators in Section 3. We numerically analyze

larger oscillator networks with STDP in Section 4. In Section 5, we numerically simulate pulse-coupled pyramidal neuron models to show that our results obtained for coupled phase oscillators qualitatively apply to spiking neuron models.

## 2 Model

We analyze a network of  $n$  phase oscillators. One oscillator is assumed not to be disturbed by the other  $n - 1$  oscillators. We designate this special oscillator as pacemaker and use the term oscillator to refer to the other  $n - 1$  elements. The pacemaker has natural frequency  $\Omega$  and phase  $\phi_0 \in [0, 2\pi)$ . The other oscillators are assumed to have the identical natural frequency  $\omega$ , and the phase of the  $i$ th oscillator ( $1 \leq i \leq n - 1$ ) is denoted by  $\phi_i \in [0, 2\pi)$ . We identify  $\phi_i = 0$  and  $\phi_i = 2\pi$  ( $0 \leq i \leq n - 1$ ). We write  $(i, j) \in E$  if there is a synaptic connection from oscillator  $i$  to oscillator  $j$ . In other words,  $E$  is the set of edges of the underlying neural network. As in real neural networks, connectivity is asymmetric in general so that  $(i, j) \in E$  does not imply  $(j, i) \in E$ . A pair of connected oscillators interact via sinusoidal coupling, which usually promotes synchrony (Kuramoto 1984).

Dynamics for fixed synaptic strengths are represented by:

$$\dot{\phi}_0 = \Omega, \tag{1}$$

$$\dot{\phi}_i = \omega + \frac{1}{\langle k \rangle} \sum_{j:(j,i) \in E} g_{ji} \sin(\phi_j - \phi_i), \quad (1 \leq i \leq n-1) \tag{2}$$

where  $\langle k \rangle$  is the average number of incoming edges per oscillator. The coupling strength  $g_{ji}$  is associated with synapse  $(j, i)$ . We note that  $g_{i0}$ , which is the synaptic weight from an oscillator to the pacemaker, does not affect the network dynamics: the pacemaker is not perturbed by external input. However, we will monitor  $g_{i0}$  to examine how this connection evolves as synaptic plasticity goes on.

We assume that  $\Omega > \omega$  unless otherwise stated. By rescaling the timescale and the coupling strength, we set  $\Omega = \omega + 1$  without losing generality. To set the values of  $\Omega$  and  $\omega$ , we take care of two subtle factors. First, a small  $\omega$  would yield backward rotation by the effect of coupling. This is because the second term of the right-hand side of Eq. (2) can be large negative to overwhelm the first term. Then, the condition  $\dot{\phi}_i < 0$  may be

satisfied for long enough time to elicit backward firing. This is unrealistic as a neuron model. Second, we avoid a pair of  $\Omega$  and  $\omega$  that accommodates the relation  $M_1\Omega = M_2\omega$  with small integers  $M_1$  and  $M_2$  ( $M_1 \neq M_2$ ). In such a situation, resonant behavior appears when the pacemaker and the oscillators are decoupled through STDP and has a pathological effect (see the explanation after Eq. (16) for more details). The resonant firing is ruled out by dynamical noise in many real neural networks. However, we have to carefully specify  $\Omega$  and  $\omega$  in the present work because we do not assume noise for analytical tractability. Keeping these caveats in mind, we set  $\Omega = 9.1$  and  $\omega = 8.1$ .

Spike time is defined to be the time when the  $\phi_i$  crosses 0. Synaptic update based on STDP takes place based on a pair of nearest presynaptic and postsynaptic spike times, without paying attention to remote spike pairs (see arguments in e.g. Froemke and Dan 2002). We compare the upshot of two types of STDP rules for synapse  $g_{ji}$  ( $(j, i) \in E$ ), namely, *asymmetric* STDP and *symmetric* STDP.

Asymmetric STDP is modeled as follows. LTP is induced if a presynaptic firing (spike of oscillator  $j$ ) precedes a postsynaptic firing (spike of oscillator  $i$ ). In the opposite case, LTD occurs. We denote the presynaptic (postsynaptic) spike time by  $t_{pre}$  ( $t_{post}$ ). A spike-pair event modifies the synaptic weight:  $g_{ji} \rightarrow g_{ji} + \Delta g_{ji}$ , where

$$\Delta g_{ji} = \begin{cases} A^+ \exp\left(-\frac{t_{post}-t_{pre}}{\tau}\right), & t_{pre} < t_{post}, \\ -A^- \exp\left(-\frac{t_{pre}-t_{post}}{\tau}\right), & t_{pre} > t_{post}. \end{cases} \tag{3}$$

under the limitation  $g_{ji} \in [0, g_{max}]$ . A sample learning window is indicated by the solid line in Fig. 1. The width of the learning window is specified by  $\tau$ , which is known to be of the order of 10–20 ms (Bi and Poo 1998; Zhang et al. 1998). We confine ourselves to the regime in which firing rates are not very large (5–20 Hz), as is true for many pyramidal neurons. Then,  $\tau$  is several times smaller than the characteristic interspike interval  $T = 50$ –200 ms. We thus set

$$\tau = \frac{1}{6} \times \frac{2\pi}{\Omega} \cong \frac{T}{6}. \tag{4}$$

For completeness, we assume that  $t_{pre} = t_{post}$  does not induce plasticity.

We assume that synaptic weights evolve so slowly that we can solve Eq. (2) by regarding the synaptic weights as constant. This assumption is valid if  $A^+\Omega, A^-\Omega \ll g^2$  for the following reason. Because the

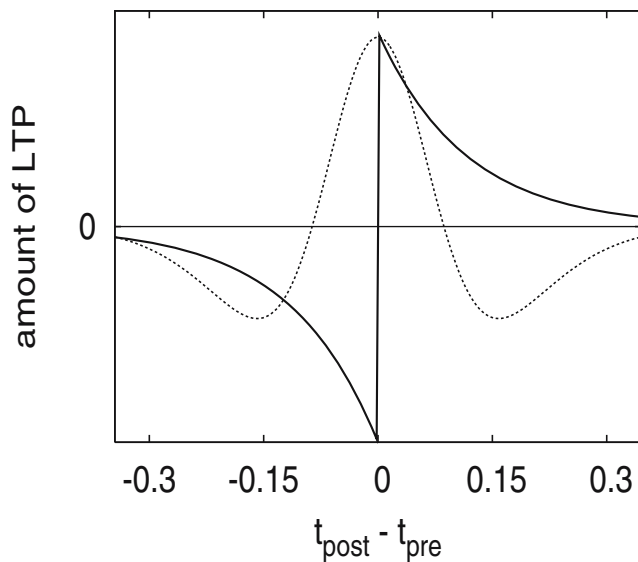


**Fig. 1** Asymmetric (solid line) and symmetric (dashed line) learning windows of STDP as a function of  $t_{post} - t_{pre}$ , namely, the postsynaptic spike time relative to the presynaptic spike time

relative phase relationship determines the evolution of synaptic weights, we should compare the typical timescale of the relative phase dynamics with that of synaptic plasticity. The former is the inverse of typical synaptic weight  $g_0$ . By introducing dimensionless synaptic weight  $g/g_0$ , we find from Eq. (3) that the timescale of dimensionless synaptic plasticity is the inverses of  $A^+\Omega/g_0$  and  $A^-\Omega/g_0$ . The two timescales are separated if  $A^+\Omega/g_0, A^-\Omega/g_0 \ll g_0$ , which leads to  $A^+\Omega, A^-\Omega \ll g_0^2 \cong g^2$ . On the slow timescale of synaptic plasticity, we can set  $A^- = 1$  by rescaling the time, so that only the ratio  $A^+/A^-$  is relevant. For the stability,  $A^+/A^-$  must be balanced. This ratio is assumed to be slightly smaller than unity according to previous literature (Song et al. 2000; Song and Abbott 2001).

Most of our theoretical efforts are invested in asymmetric STDP because many pyramidal neurons show asymmetric STDP. However, symmetric STDP, in which the synaptic update rule depends only on  $|t_{pre} - t_{post}|$ , is also found in some experiments. Particularly, the learning window is often shaped like a mexican hat in excitatory synapses; small (large)  $|t_{pre} - t_{post}|$  induces LTP (LTD) (Nishiyama et al. 2000; Abbott and Nelson 2000; Shouval et al. 2002). Symmetric learning windows have been found for inhibitory synapses (Woodin et al. 2003) and for the amount of LTD in excitatory synapses (Dan and Poo 1992). We numerically analyze networks with symmetric STDP in Section 4. We adopt superposition of two gaussian distributions as the symmetric learning window, as depicted by the dotted line in

Fig. 1. A spike-pair event modifies the synaptic weight:  $g_{ji} \rightarrow g_{ji} + \Delta g_{ji}$ , where

$$\Delta g_{ji} = \frac{A^+}{\sqrt{2\pi\sigma^{+2}}} \exp\left(-\frac{(t_{pre} - t_{post})^2}{2\sigma^{+2}}\right) - \frac{A^-}{\sqrt{2\pi\sigma^{-2}}} \exp\left(-\frac{(t_{pre} - t_{post})^2}{2\sigma^{-2}}\right), \quad (5)$$

with  $\sigma^+ < \sigma^-$ . We set  $\sigma^+ = 0.6\tau$  and  $\sigma^- = 2\sigma^+ = 1.2\tau$  so that the timescale of the symmetric learning window is comparable to that of the asymmetric learning window defined in Eq. (3). The values of  $A^+$  and  $A^-$  are assumed to be the same as those for asymmetric STDP so that  $g_{ji}$  is bounded.

### 3 Analysis of small networks with asymmetric STDP

We begin with small networks of two oscillators with asymmetric STDP. For these networks, how much initial coupling is necessary for synchrony can be analytically evaluated.

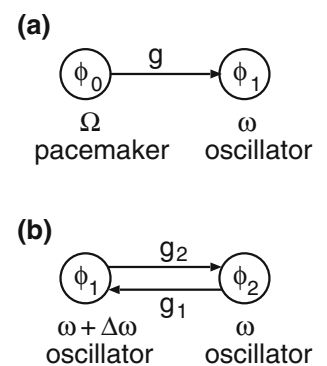
#### 3.1 One pacemaker and one oscillator

We deal with the case  $n = 2$ , namely, a network of one pacemaker and one oscillator. Because the connection from the oscillator to the pacemaker does not affect the dynamics of the pacemaker, it suffices to consider the unidirectional case. The network is schematically shown in Fig. 2(a). We write  $g = g_{01}$  to simplify the notation. The short-term dynamics in which  $g$  is regarded to be constant are described by

$$\dot{\phi}_0 = \Omega, \quad (6)$$

$$\dot{\phi}_1 = \omega + g \sin(\phi_0 - \phi_1). \quad (7)$$

**Fig. 2** Schematic diagrams showing (a) the network of one pacemaker and one oscillator, and (b) the network of two oscillators



With  $\psi \equiv \phi_0 - \phi_1$ , Eqs. (6) and (7) reduce to

$$\dot{\psi} = \Omega - \omega - g \sin \psi. \tag{8}$$

Based on the assumption that synaptic plasticity occurs much more slowly than firing, we perform quasistatic analysis. For a frozen  $g$ , let us derive the average angular frequency of the oscillator denoted by  $\tilde{\omega}$ . If  $g \geq \Omega - \omega$ , the pacemaker and the oscillator are in frequency synchrony, i.e.  $\tilde{\omega} = \Omega$ . If  $0 \leq g < \Omega - \omega$ , Eq. (8) is equivalent to

$$\int \frac{d\psi}{\Omega - \omega - g \sin \psi} = \int dt. \tag{9}$$

Integration of Eq. (9) over a cycle yields

$$\begin{aligned} \frac{2\pi}{\Omega - \tilde{\omega}} &= \int_0^T dt = \int_0^{2\pi} \frac{d\psi}{\Omega - \omega - g \sin \psi} \\ &= \frac{2\pi}{\sqrt{(\Omega - \omega)^2 - g^2}}, \end{aligned} \tag{10}$$

which results in

$$\tilde{\omega} = \Omega - \sqrt{(\Omega - \omega)^2 - g^2}. \tag{11}$$

Note that  $\omega \leq \tilde{\omega} < \Omega$ .

The direction and the amount of synaptic plasticity induced by a single spike-pair event is determined by  $t_{post} - t_{pre}$ . We estimate  $t_{post} - t_{pre}$  in terms of  $\psi$  as follows. Suppose that the phase difference is equal to  $\psi$  when the pacemaker fires. Then, it approximately takes  $t_{post} - t_{pre} = \psi/\tilde{\omega}$  for the oscillator to fire. In this case, LTP is induced because the pacemaker is presynaptic to the oscillator. The pacemaker and the oscillator can fire in the opposite order. If the phase difference is  $\psi$  when the oscillator fires prior to the pacemaker does, the pacemaker spends approximately  $t_{post} - t_{pre} = \psi/\Omega$  before firing. In this case, LTD is induced. Because we confine ourselves to the case in which  $\Omega$  does not deviate so much from  $\omega$ , we approximate  $t_{post} - t_{pre} \cong \psi/\Omega$  regardless of the order of firing.

In Eq. (4), we assumed that the decay rate of the learning window  $\tau$  is sufficiently smaller than  $T/2$ ,

which corresponds to phase  $\pi$ . Therefore, the amount of LTP is negligible for  $t_{post} - t_{pre} \cong \pi/\tilde{\omega}$  or larger, and the LTP rule is effective only when  $0 < \psi \leq \pi$ . By the same token, the LTD rule is effective only for  $-\pi < \psi < 0$ . Using these approximations, we aim to describe the dynamics of synaptic plasticity in terms of phase variables. The amount of plasticity given by Eq. (3) can be rewritten as

$$\Delta g = \begin{cases} A^+ \exp\left(-\frac{\psi}{\Omega\tau}\right), & 0 < \psi \leq \pi, \phi_1 = 0 \\ -A^- \exp\left(\frac{\psi}{\Omega\tau}\right), & -\pi < \psi < 0, \phi_0 = 0 \end{cases} \tag{12}$$

where  $\phi_1 = 0$  and  $\phi_0 = 0$  indicate the postsynaptic spike time for an LTP event (the spike time of the oscillator) and that of an LTD event (the spike time of the pacemaker), respectively.

We denote by  $g(0)$  the initial synaptic weight. If  $g(0) \geq \Omega - \omega$ , fast dynamics have two steady states given by

$$\psi^* = \arcsin\left(\frac{\Omega - \omega}{g(0)}\right). \tag{13}$$

The solution with  $\pi/2 < \psi^* \leq \pi$  is unstable, and hence the fast dynamics converges to  $\psi^*$  satisfying  $0 \leq \psi^* \leq \pi/2$ . Therefore, STDP induces potentiation of  $g$ . Then,  $\psi^*$  for an altered  $g$  becomes even smaller, which induces further potentiation of  $g$ . Eventually,  $g = g_{max}$  is achieved. In sum, if

$$g(0) \geq g_c \equiv \Omega - \omega, \tag{14}$$

the pacemaker and the oscillator will synchronize quickly without plasticity. The STDP does not break frequency synchrony. Note that STDP generally decreases the phase difference  $\psi$ , but  $\psi$  does not tend to 0 (no phase synchrony) unless  $\Omega = \omega$ . Alternatively, if  $g_{max} = \infty$ ,  $g$  diverges, and  $\psi$  goes to 0.

Does asymmetric STDP facilitate frequency synchrony? If  $g(0) < g_c$ , the oscillator is initially not entrained by the pacemaker. Then,  $\psi$  slips. By averaging over many spike-pair events, we represent the synaptic dynamics on a slow timescale by

$$\dot{g} = \frac{\tilde{\omega}}{2\pi} \left[ \int_t \text{such that } 0 < \psi < \pi A^+ e^{-\psi/\Omega\tau} dt - \int_t \text{such that } -\pi < \psi < 0 A^- e^{-\psi/\Omega\tau} dt \right] \tag{15}$$

$$\propto \int_0^\pi e^{-\psi/\Omega\tau} \left( \frac{A^+}{g_c - g \sin \psi} - \frac{A^-}{g_c + g \sin \psi} \right) d\psi. \tag{16}$$

Derivation of Eq. (15) requires the nonresonant situation. If  $M_1\Omega = M_2\omega$  holds with small  $M_1$  and  $M_2$ , the dynamics become periodic with a rather small period when the oscillator decouples from the pacemaker due to STDP. If this were the case, the dependence on the initial condition does not vanish permanently. In other words,  $\psi$  conditioned by  $\phi_0 = 0$  or  $\phi_1 = 0$  in Eq. (12) would take only limited values. Then the distribution of  $\psi$  conditioned by a spike event would deviate from the unconditioned distribution of  $\psi$ . With our choice of  $\Omega = 9.1$  and  $\omega = 8.1$ , the effect of such a resonance is very small.

In the region of  $g$  where  $\dot{g} > 0$  holds, the RHS of Eq. (16) increases monotonically with  $g$ . If  $g(0)$  is greater than the value that makes the RHS equal to zero, which we denote by  $g_{c-stdp}$ , we obtain  $\dot{g} > 0$ . Under this condition,  $g$  continues to increase, and  $\psi^*$  decreases. This makes  $\dot{g}$  in Eq. (16) even larger. This positive feedback lasts until  $g \geq g_c$  is eventually satisfied. As a result, frequency synchrony is elicited by STDP. However, if  $g(0) < g_{c-stdp}$ ,  $g$  converges to the lower bound 0, so that the oscillator is disconnected from the pacemaker.

We bound  $g_{c-stdp}$  as follows:

$$\begin{aligned} \text{RHS of Eq. (16)} &= \int_0^\pi e^{-\psi/\Omega\tau} \left[ \frac{A^+}{g_c} \frac{1}{1 - \frac{g \sin \psi}{g_c}} - \frac{A^-}{g_c} \left( 1 - \frac{\frac{g \sin \psi}{g_c}}{1 + \frac{g \sin \psi}{g_c}} \right) \right] \\ &\geq \int_0^\pi e^{-\psi/\Omega\tau} \left[ \frac{A^+}{g_c} \left( 1 + \frac{g \sin \psi}{g_c} \right) - \frac{A^-}{g_c} \left( 1 - \frac{g \sin \psi}{g_c} \frac{1}{1 + \frac{g}{g_c}} \right) \right] d\psi \\ &= -\frac{A^- - A^+}{g_c} \int_0^\pi e^{-\psi/\Omega\tau} d\psi + \frac{g}{g_c^2} \left( A^+ + \frac{A^-}{1 + \frac{g}{g_c}} \right) \int_0^\pi e^{-\psi/\Omega\tau} \sin \psi d\psi \\ &= -\frac{(A^- - A^+)\Omega\tau(1 - e^{-\pi/\Omega\tau})}{g_c} + \frac{g}{g_c^2} \frac{A^+ + A^-}{1 + \frac{g}{g_c}} \frac{\Omega^2\tau^2(1 + e^{-\pi/\Omega\tau})}{1 + \Omega^2\tau^2}. \end{aligned} \quad (17)$$

The value of  $g$  that makes the RHS of the above equation zero gives an upper bound of  $g_{c-stdp}$ . When  $A^+$  and  $A^-$  are balanced ( $A^+ \cong A^-$ ), we obtain

$$\begin{aligned} g_{c-stdp} &\leq \frac{\frac{A^- - A^+}{A^- + A^+} \frac{(1 + \Omega^2\tau^2)(1 - e^{-\pi/\Omega\tau})}{\Omega\tau(1 + e^{-\pi/\Omega\tau})}}{1 - \frac{A^- - A^+}{A^- + A^+} \frac{(1 + \Omega^2\tau^2)(1 - e^{-\pi/\Omega\tau})}{\Omega\tau(1 + e^{-\pi/\Omega\tau})}} g_c \\ &\cong \frac{A^- - A^+}{A^- + A^+} \frac{(1 + \Omega^2\tau^2)(1 - e^{-\pi/\Omega\tau})}{\Omega\tau(1 + e^{-\pi/\Omega\tau})} g_c. \end{aligned} \quad (18)$$

Because  $\Omega\tau$  is assumed to be of the order of  $\pi$  (see Eq. (4)),  $\Omega\tau = O(1)$ . In addition, when  $A^+ \cong A^-$ , the inequalities in Eqs. (17) and (18) nearly hold with the equalities. In such a case,

$$g_{c-stdp} \propto \left( 1 - \frac{A^+}{A^-} \right) g_c, \quad (19)$$

which implies that  $g_{c-stdp}$  is much smaller than  $g_c$  when  $A^+ \cong A^-$ . Particularly,  $g_{c-stdp}$  is extinguished when  $A^+ \geq A^-$ .

In Fig. 3, we plot  $g_{c-stdp}$  evaluated by numerical integration of Eq. (16) and the approximation given by Eq. (18). We also plot  $g_{c-stdp}$  obtained by numerical simulations of our model Eqs. (3, 6), and (7), in which  $g_{c-stdp}$  is determined by varying the initial synaptic weight  $g(0)$ . The evaluation by Eq. (16) (solid line) is in good agreement with  $g_{c-stdp}$  obtained by numerical simulations of the model (circles) for a broad range of  $A^+/A^-$ . As expected, the approximate estimation by Eq. (18) (dotted line) also agrees with the numerical data (circles) when  $A^+/A^-$  is close to unity. In conclusion, asymmetric STDP drastically enhances frequency synchrony.

Regarding symmetric STDP, for values of  $g$  such that  $\psi$  falls in the positive learning window (refer to the dotted line in Fig. 1),  $g$  is strengthened to eventually exceed  $g_c$ . Therefore, frequency synchrony is facilitated. To what extent synchrony is promoted depends on the width of the learning window.

When  $\Omega < \omega$ , there are two solutions  $\psi^* \in (-\pi, 0)$ , one of which is stable. Then, STDP elicits LTD. Even though  $\psi^*$  changes, the relation  $-\pi < \psi^* < 0$  is

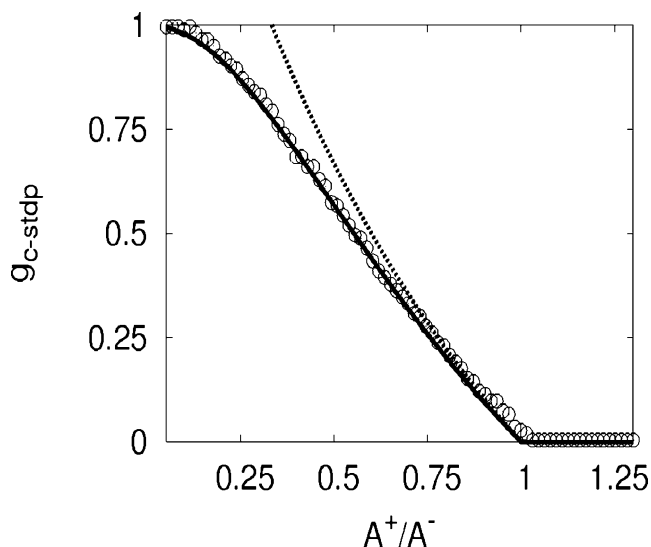


**Fig. 3**  $g_{c-stdp}$  for the network with one pacemaker and one oscillator. The evaluation by Eq. (16) (solid line), that by Eq. (18) (dotted line), and  $g_{c-stdp}$  determined by numerical simulations of the coupled phase oscillators (circles) are compared. We set  $g_{max} = 1.25$

preserved until the pacemaker and the oscillator get disconnected. As a result, frequency synchrony does not happen.

### 3.2 Two oscillators

To examine how the connectivity between a pair of oscillators evolves in a large network, we analyze the following toy model of two bidirectionally coupled oscillators:

$$\begin{aligned} \dot{\phi}_1 &= \omega + \Delta\omega + g_1 \sin(\phi_2 - \phi_1), \\ \dot{\phi}_2 &= \omega + g_2 \sin(\phi_1 - \phi_2), \end{aligned} \tag{20}$$

where  $g_1, g_2 \in [0, g_{max}]$ . The network is depicted in Fig. 2(b). Now two oscillators influence each other, which contrasts to the case of the pacemaker-oscillator network examined in Section 3.1. The term  $\Delta\omega$  represents the mismatch in natural frequencies. Although the oscillators are identical in our original model (see Eq. (2)), we introduce  $\Delta\omega$  because of the following reason. In oscillator networks with a pacemaker, the oscillators are not completely phase synchronized. The oscillators directly connected to the pacemaker are the first to fire after the pacemaker does. Then, other oscillators adjacent to those connected to the pacemaker fire after some delay, and so forth. Therefore, the

oscillators closer to the pacemaker tend to have more advanced phases, and the distribution of the phases is associated with the hierarchical organization of the network. Imagine two oscillators coupled unidirectionally or bidirectionally in a large network. We denote one that fires first and the other by oscillators 1 and 2 respectively. Precisely, the difference in the firing timing stems from complex effects of coupling with other oscillators. For analytical tractability, here we replace such effects by the frequency mismatch  $\Delta\omega$ , by which the difference in the firing timing can be easily introduced. As shown in the following, for  $\Delta\omega > 0$ , oscillator 1 tends to fire in advance of oscillator 2. Accordingly, we regard that oscillator 1 is closer to the pacemaker than oscillator 2.

We analyze the model given by Eq. (20). By introducing  $\psi \equiv \phi_1 - \phi_2$ , we derive

$$\dot{\psi} = \Delta\omega - (g_1 + g_2) \sin \psi. \tag{21}$$

If

$$g_1(0) + g_2(0) \geq \Delta\omega, \tag{22}$$

two oscillators are locked with phase lag  $0 < \psi^* < \pi/2$ , where

$$\psi^* = \arcsin\left(\frac{\Delta\omega}{g_1 + g_2}\right). \tag{23}$$

If synaptic plasticity is absent, Eq. (22) gives the condition for frequency synchrony.

In contrast to the network of one pacemaker and one oscillator analyzed in Section 3.1, Eq. (22) does not guarantee that frequency synchrony is maintained throughout STDP. When Eq. (22) is satisfied, the synaptic dynamics are written as

$$\dot{g}_1 = -A^- \exp\left(-\frac{\psi^*}{\tilde{\omega}\tau}\right), \tag{24}$$

$$\dot{g}_2 = A^+ \exp\left(-\frac{\psi^*}{\tilde{\omega}\tau}\right), \tag{25}$$

where

$$\tilde{\omega} = \omega + \frac{g_2 \Delta\omega}{g_1 + g_2} \tag{26}$$

is the frequency common to the two oscillators. Because  $A^+ < A^-$ ,  $g_1 + g_2$  decreases with time. The oscillators desynchronize in frequency if  $g_1 + g_2 \geq \Delta\omega$  is violated via synaptic plasticity. For sufficiently small  $g_1(0) + g_2(0)$ , the two oscillators are disconnected even from the beginning. In these cases,  $\psi$  slips due to the absence of frequency synchrony.

The average frequencies of the two oscillators out of frequency synchrony are calculated as

$$\tilde{\omega}_1 = \omega + \frac{g_2\Delta\omega + g_1\sqrt{\Delta\omega^2 - (g_1 + g_2)^2}}{g_1 + g_2}, \quad (27)$$

$$\tilde{\omega}_2 = \omega + \frac{g_2\Delta\omega - g_1\sqrt{\Delta\omega^2 - (g_1 + g_2)^2}}{g_1 + g_2}. \quad (28)$$

The synaptic weights evolve according to

$$\begin{aligned} \dot{g}_1 &= \frac{1}{2\pi} \int_0^\pi \left[ \frac{A^+ e^{-\psi/\tilde{\omega}_1\tau}}{\Delta\omega + (g_1 + g_2) \sin \psi} - \frac{A^- e^{-\psi/\tilde{\omega}_2\tau}}{\Delta\omega - (g_1 + g_2) \sin \psi} \right] d\psi \\ &= \frac{1}{2\pi} \int_0^\pi e^{-\psi/\tilde{\omega}_1\tau} \left[ \frac{A^+}{\Delta\omega + (g_1 + g_2) \sin \psi} - \frac{A^-}{\Delta\omega - (g_1 + g_2) \sin \psi} \right] d\psi, \end{aligned} \quad (29)$$

$$\begin{aligned} \dot{g}_2 &= \frac{1}{2\pi} \int_0^\pi \left[ \frac{A^+ e^{-\psi/\tilde{\omega}_2\tau}}{\Delta\omega - (g_1 + g_2) \sin \psi} - \frac{A^- e^{-\psi/\tilde{\omega}_1\tau}}{\Delta\omega + (g_1 + g_2) \sin \psi} \right] d\psi \\ &= \frac{1}{2\pi} \int_0^\pi e^{-\psi/\tilde{\omega}_1\tau} \left[ \frac{A^+}{\Delta\omega - (g_1 + g_2) \sin \psi} - \frac{A^-}{\Delta\omega + (g_1 + g_2) \sin \psi} \right] d\psi, \end{aligned} \quad (30)$$

where we approximated  $e^{-\psi/\tilde{\omega}_2\tau}$  by  $e^{-\psi/\tilde{\omega}_1\tau}$ , as we did in Section 3.1.

Since  $\dot{g}_1 < 0$  is always satisfied,  $g_1$  eventually reaches 0; backward connectivity from a downstream oscillator to an upstream oscillator is eliminated. Whether a ‘forward’ connectivity from the upstream oscillator to the downstream oscillator survives relies on  $g_2(\hat{t})$  where  $\hat{t}$  is the time  $g_1$  reaches 0. If  $g_2(\hat{t})$  is larger than  $g_{c-stdp}$  obtained in Section 3.1, frequency synchrony will be eventually established. In this case, the final oscillation

frequency is equal to  $\omega + \Delta\omega$  so that oscillator 2 is enslaved by oscillator 1. If  $g_2(\hat{t}) < g_{c-stdp}$ , the two oscillators are finally disconnected.

The critical value of  $g_2(0)$  above which frequency synchrony occurs is plotted in Fig. 4 for different values of  $A^+/A^-$  and  $g_1(0)$ . The critical  $g_2(0)$  decreases with  $g_1(0)$ , implying that a large  $g_1(0)$  enhances frequency synchrony. Such backward connectivity transiently serves to keep  $\psi$  small so that forward connectivity is enhanced. However, only the synapse from the faster oscillator to the slower oscillator survives eventually.

The feedforward network is not created via symmetric STDP, by which  $g_1$  and  $g_2$  evolve in the same direction. When initial mutual connectivity is strong enough, synchrony is established so that the two synaptic weights are saturated ( $g_1 = g_2 = g_{max}$ ). Then, based on Eq. (26), the common firing frequency is equal to  $\omega + \Delta\omega/2$ , but not to the frequency of the faster oscillator ( $= \omega + \Delta\omega$ ).

The effect of LTP-LTD balance is also shown in Fig. 4. When  $A^+$  is close to  $A^-$ , critical  $g_2(0)$  is lowered, and entrainment occurs easily. Even when LTP is rather weak compared to LTD ( $A^+/A^- = 0.8$ , thinnest line), the critical  $g_2$  is much reduced from  $g_c$ .

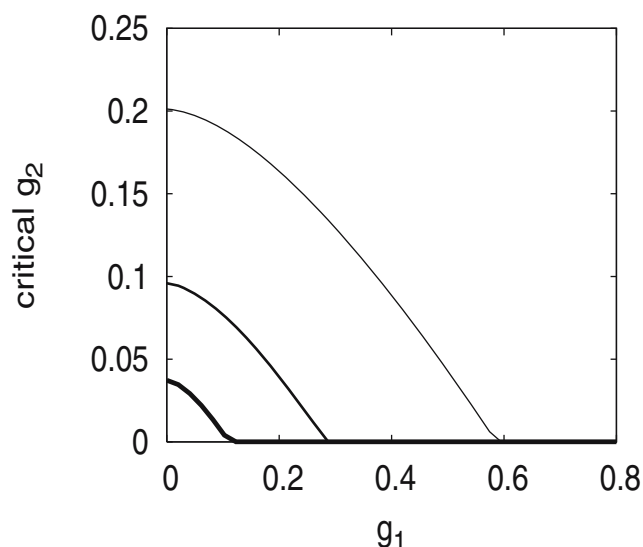


**Fig. 4** The critical  $g_2(0)$  as a function of  $g_1(0)$  for the network with two oscillators (and no pacemaker). Three lines correspond to  $A^+/A^- = 0.96$  (thickest line), 0.9, and 0.8 (thinnest line)

#### 4 Numerical results for large networks

So far, we have analyzed small networks composed of two elements only. In this section, we examine how

frequency synchrony can be facilitated by STDP in larger networks. In particular, we compare  $g_c$  and  $g_{c-stdp}$  and also investigate evolution of network structure. To this end, we numerically simulate randomly connected  $n = 100$  elements (99 oscillators and one pacemaker) based on Eqs. (3, 6), and (7).

### 4.1 Initial setup

We generate a directed random network as follows. Starting from a set of  $n$  isolated vertices, we add a directed edge that connects a randomly chosen pair of oscillators. We forbid multiple directed edges between a pair of oscillators and self loops, i.e. edges whose origin and destination are identical. This procedure is repeated  $n \langle k \rangle$  times. In the following, we assume that  $\langle k \rangle = 10$ . In other words, each oscillator is presynaptic to 10 other oscillators and postsynaptic to the same number of oscillators on average.

We define the distance  $l_i$  of oscillator  $i$  from the pacemaker by the smallest number of directed edges necessary to reach from the pacemaker to oscillator  $i$ . For example, the number of the oscillators at distance 1 is equal to those that receive direct synaptic contacts from the pacemaker. Therefore, about  $\langle k \rangle$  oscillators have distance 1. Among the other oscillators, those receiving an edge from an oscillator with distance 1 have distance 2. The depth  $L$  of a network is defined as the distance averaged over all the oscillators:  $L = \sum_{i=1}^{n-1} l_i / (n - 1)$ .

The initial phases  $\phi_i$  ( $0 \leq i \leq n - 1$ ) are taken independently from the uniform density on  $[0, 2\pi)$ . For all the synapses, we initially set  $g_{ji} = g(0)$ .

For a specific random network used in the following numerical simulations, we obtained  $L = 3.22$ . For this network, we numerically found that frequency synchrony happens without synaptic plasticity if  $g \geq g_c \cong 100.7$ . In this case, the pacemaker first fires in each cycle, and oscillators with smaller distances tend to fire with smaller lag with respect to the pacemaker (Kori and Mikhailov 2004).

### 4.2 Measured quantities

We define the degree of frequency synchrony  $r \equiv r([t_1, t_2])$  for a time interval  $[t_1, t_2]$ . The mean frequency of each oscillator for this time interval is equal to

$$\tilde{\omega}_i = \frac{\phi_i(t_2) - \phi_i(t_1)}{t_2 - t_1}. \tag{31}$$

We note that  $\tilde{\omega}_0 = \Omega$ . Then, the synchrony measure is defined by

$$r = \frac{\frac{1}{n-1} \sum_{i=1}^{n-1} \tilde{\omega}_i - \omega}{\Omega - \omega}. \tag{32}$$

When the oscillators are in frequency synchrony with the pacemaker, the mean frequency of the oscillators  $\sum_{i=1}^{n-1} \tilde{\omega}_i / (n - 1)$  is equal to the frequency of the pacemaker  $\Omega$ , and we have  $r = 1$ . If the pacemaker does not at all affect the other  $n - 1$  oscillators, the oscillators fire at their natural frequency  $\omega$ , and we have  $r = 0$ . We divide the total simulation time into consecutive bins of the width  $t_2 - t_1 = 100$  for oscillator simulations in Sections 4.3 and 4.4.

More microscopically, we inspect possible formation of feedforward chains originating from the pacemaker. To quantify this, we track several order parameters derived from synaptic weights. The first is the depth  $L$  extended to networks with heterogeneous synaptic weights in the following way. Let us consider a path from the pacemaker to oscillator  $i$ . A path is equivalent to a chain of directed synapses:  $(j_0, j_1) \in E, (j_1, j_2) \in E, \dots, (j_{k_i-1}, j_{k_i}) \in E$ , where  $j_0 = 0$  and  $j_{k_i} = i$ . The length of this path is given by  $\sum_{k=0}^{k_i-1} g_{max} / g_{j_k j_{k+1}}$ . The distance  $l_i$  of oscillator  $i$  from the pacemaker is the shortest path length among all possible paths from the pacemaker to oscillator  $i$  (Braunstein et al. 2003). This definition generalizes the prior definition for networks with unit synaptic weights. The redefined distance is associated with how much a downstream oscillator is influenced by the pacemaker. The depth of the network is again defined by  $L = \sum_{i=1}^{n-1} l_i / (n - 1)$  and measures effective proximity of the oscillators from the pacemaker. By definition, the generalized  $L$  is equal to or larger than  $L$  of the unweighted network, with equality realized only when  $g_{ji} = g_{max}$  for all the synapses that appear in the shortest paths.

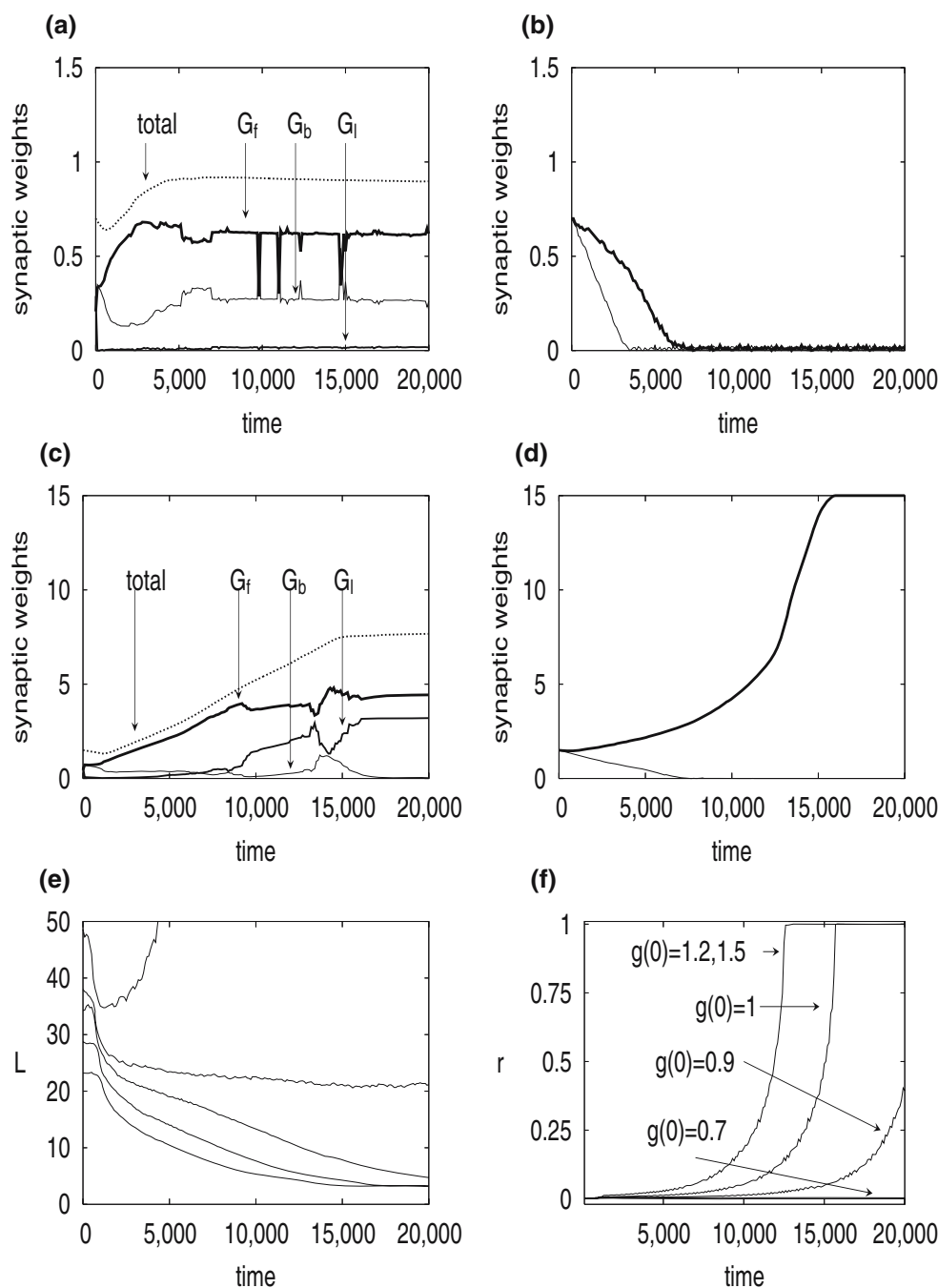
A synaptic connection  $(j, i)$  with  $l_j < l_i$  ( $l_j > l_i$ ) is a forward (backward) connection in the meaning that it complies with the feedforward chain emanating from the pacemaker. Accordingly, we define the amount of forward connection  $w_f$ , that of backward connection  $w_b$ , and that of lateral connection  $w_l$  by

$$G_f = \sum_{l_i - l_j > \epsilon} \frac{g_{ji}}{n \langle k \rangle}, \tag{33}$$

$$G_b = \sum_{l_i - l_j < -\epsilon} \frac{g_{ji}}{n \langle k \rangle}, \tag{34}$$

$$G_l = \sum_{-\epsilon \leq l_i - l_j \leq \epsilon} \frac{g_{ji}}{n \langle k \rangle}. \tag{35}$$

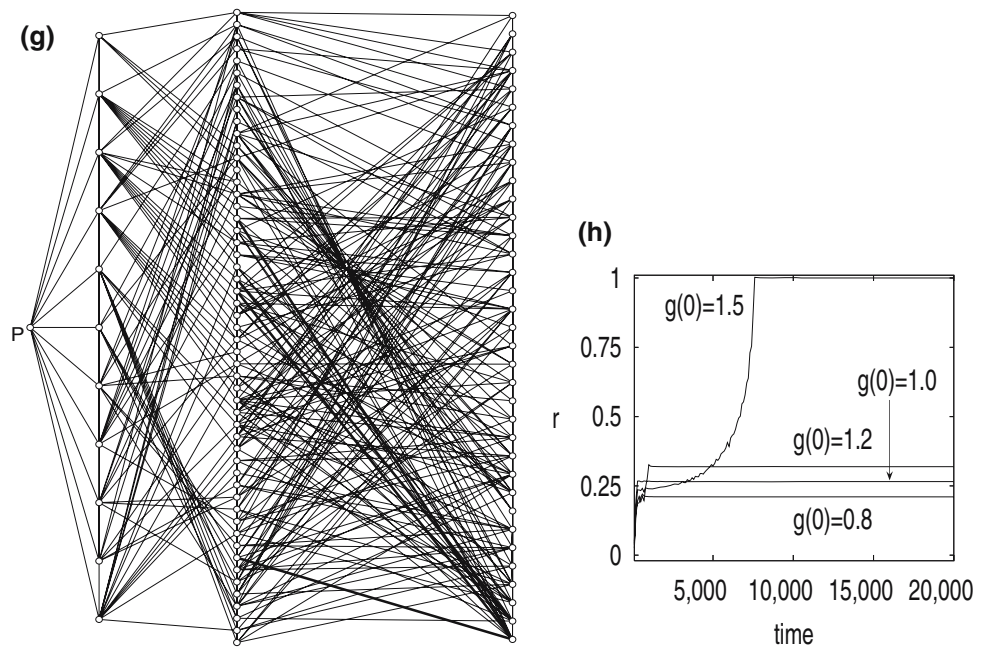
**Fig. 5** Results for 100 randomly coupled oscillators subject to asymmetric STDP. Evolution of the synaptic-weight order parameters are shown for (a, b)  $g(0) = 0.7$  and (c, d)  $g(0) = 1.5$ . In (a) and (c),  $G_f$  (thick solid lines),  $G_b$  (thin solid lines),  $G_l$  (moderate solid lines), and the average weight (dotted lines) are shown. In (b) and (d),  $G_f^0$  (thick lines) and  $G_b^0$  (thin lines) are indicated. Time courses of (e)  $L$  and (f)  $r$  are compared for  $g(0) = 0.7, 0.9, 1, 1.2,$  and  $1.5$ . In (e), lower lines correspond to larger  $g(0)$ . (g) Final network structure for  $g(0) = 1.5$ . Only the synapses  $(j, i) \in E$  with  $g_{ji} > g(0)$  are presented. The pacemaker is labeled  $P$ . Forward edges and backward edges are indicated by thin lines and thick lines, respectively. The network is drawn by Pajek (<http://vlado.fmf.uni-lj.si/pub/networks/pajek/>). (h) Time courses of  $r$  for some values of  $g(0)$  when the oscillators are heterogeneous



Summation is taken over the pairs of oscillators forming synapses  $((j, i) \in E)$ . Note that  $G_l$  quantifies the connection between oscillators whose distances from the pacemaker are approximately equal. The number of synapses in the network  $(= n \langle k \rangle)$  gives normalization, and thus  $0 \leq G_f, G_b, G_p \leq g_{max}$ . The average synaptic weight is given by  $0 \leq G_f + G_b + G_p \leq g_{max}$ . The tolerance level is chosen to be sufficiently small:  $\epsilon = 0.05$ .

We also define local quantities to evaluate feedforwardness. The average weight of the synapses postsynaptic to the pacemaker is denoted by  $G_f^0$ . This is equal to the average of  $g_{0i}$  over  $i$  with  $(0, i) \in E$ . This corresponds to  $g$  used in Section 3.1. Similarly, the average weight of the synapses presynaptic to the pacemaker is denoted by  $G_b^0$ . This is equal to the average of  $g_{i0}$  over  $i$  with  $(i, 0) \in E$ . We note that  $0 \leq G_f^0, G_b^0 \leq g_{max}$ .

Fig. 5 continued



### 4.3 Asymmetric learning window

We apply asymmetric STDP with LTD slightly stronger than LTP (Song et al. 2000; Song and Abbott 2001):  $A^+ = 0.009$  and  $A^- = 0.01$ . By setting  $g_{max} = 15 < g_c$ , homogeneous enhancement of all the synapses does not lead to synchrony. We determine  $g_{c-stdp}$  by running numerical simulations with various values of the initial synaptic weight  $g_{ji} = g(0)$ .

Because  $A^+$  is close to  $A^-$ , our results in Section 3 predict the following.

- As shown in Section 3.2, backward connection will be eliminated via the asymmetric STDP so that  $G_b$  and  $G_b^0$  decrease.
- The unidirectional connection between the pacemaker and the oscillator will be easily established (Section 3.1). As a result, a feedforward chain rooted at the pacemaker is expected to form.
- $g_{c-stdp}$  is much smaller than  $g_c$ .

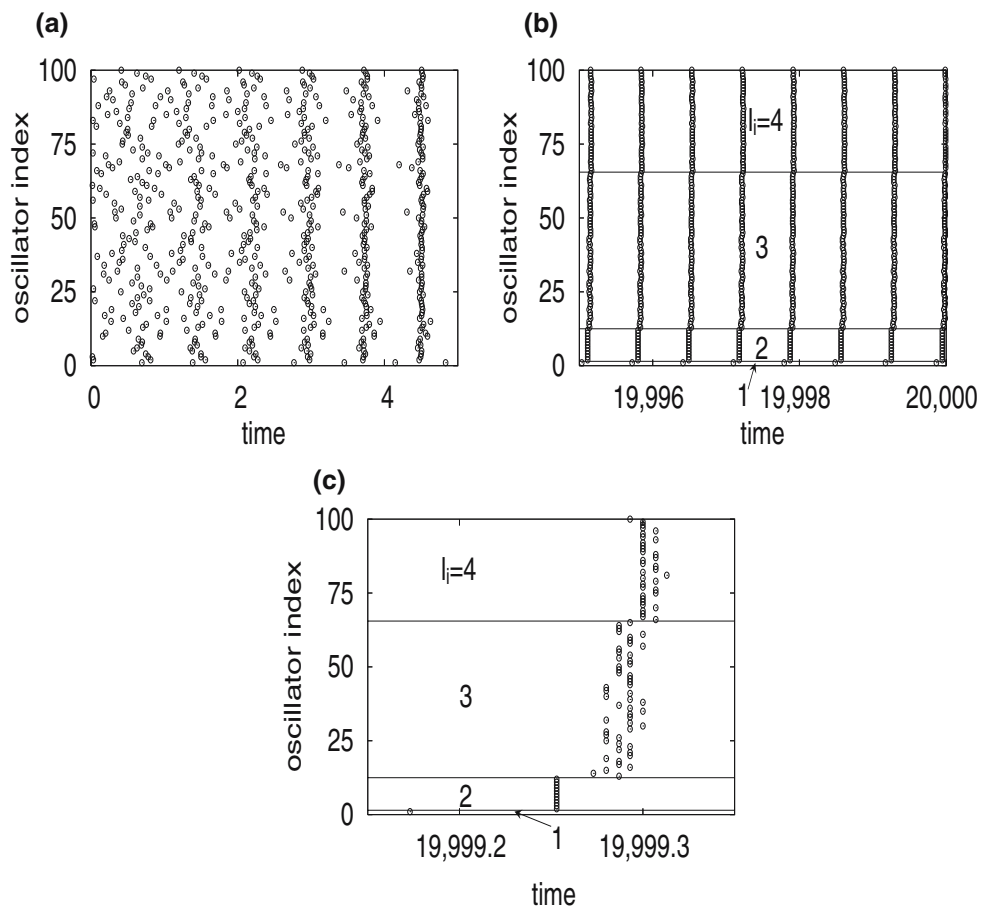
Dynamics of synaptic-weight order parameters for  $g(0) = 0.7$  are shown in Fig. 5(a, b). The average synaptic weight (dotted line in Fig. 5(a)) increases in the initial stage because some synapses between the oscillators are potentiated. However, its stationary value is much smaller than the maximal possible value ( $g_{max} = 15$ ). There is no selective potentiation of forward synapses ( $G_f$ , thick solid line in Fig. 5(a)) or depression of backward synapses ( $G_b$ , thin solid line

in Fig. 5(a)). The forward connectivity from the pacemaker ( $G_f^0$ , thick line in Fig. 5(b)) also degrades with time. Eventually, the oscillators disconnect from the pacemaker, which is observed as indefinitely growing  $L$  (uppermost line in Fig. 5(e)). Accordingly, frequency synchrony between the pacemaker and the oscillators is not achieved; Fig. 5(f) indicates that  $r$  stays near 0.

By contrast, frequency synchrony without phase synchrony is established when  $g(0) = 1.5$ , as supported by the rastergrams in Figs. 6(a) and 6(b) corresponding to initial and final periods of simulations, respectively. More in detail, forward connectivity  $G_f$  (thick solid line in Fig. 5(c)) and  $G_f^0$  (thick line in Fig. 5(d)) grow toward  $g_{max}$  to result in frequency synchrony at  $t \cong 12500$  (Fig. 5(f)), accompanied by a decrease in  $L$  (lowermost line in Fig. 5(e)). Backward synapses directly projecting to the pacemaker are pruned in an initial stage ( $G_b^0$ ; thin line in Fig. 5(d)). It takes longer time for  $G_b$  to decay (thin solid line in Fig. 5(c)). Although randomness in the initial condition blurs the phase transition, we estimate  $g_{c-stdp} \cong 0.9$  based on Fig. 5(e) and (f). Consistent with the results in Section 3.1,  $g_{c-stdp}$  is much smaller than  $g_c \cong 100.7$ .

Frequency synchrony is made possible by combined effects of sufficiently large forward weights and sufficiently small backward weights. It is not an immediate consequence of increased average synaptic weights; achieving synchrony merely by homogeneously strong synapses necessitates  $G_f + G_b + G_p \geq g_c$ . Because of

**Fig. 6** Rastergrams of the oscillators under asymmetric STDP in **(a)** initial and **(b)** final cycles. We set  $g(0) = 1.5$ . The oscillators are aligned according to their distances  $l_i$  from the pacemaker, which is calculated at time 0 in **(a)** and 19,995 in **(b)**. After sufficient time,  $l_i$  is quantized, and the values of  $l_i$  are shown in **(b)**. **(c)** is a magnification of **(b)**



our choice of  $g_{max} (< g_c)$ , homogeneous LTP does not induce frequency synchrony. Elimination of backward weights is essential for frequency synchrony. The final network structure reconstructed from synapses with  $g_{ji} > g(0) = 1.5$  is shown in Fig. 5(g), with forward and backward edges shown by thin and thick lines, respectively. Few backward edges survive asymmetric STDP. The network is close to a feedforward network rooted at the pacemaker, which enslaves the oscillators.

We remark that detailed behavior of the network order parameters varies according to the value of  $\epsilon$  and the definition of the distance  $l_i$ , which is inherently arbitrary for weighted networks. However, the general tendency that forward synapses are potentiated and backward synapses are depressed for  $g \geq g_{c-stdp}$  is observed irrespective of these details. For a reasonably defined  $l_i$ , whether  $L$  increases or decreases (Fig. 5(e)) and whether feedforward networks form (Fig. 5(g)) are determined independently of the definition of  $l_i$ .

We have performed additional numerical simulations in which every presynaptic spike spends for  $\tau/5 = T/30$  before exciting the postsynaptic neurons. Because  $T = 50\text{--}200$  ms, the corresponding synaptic delay is

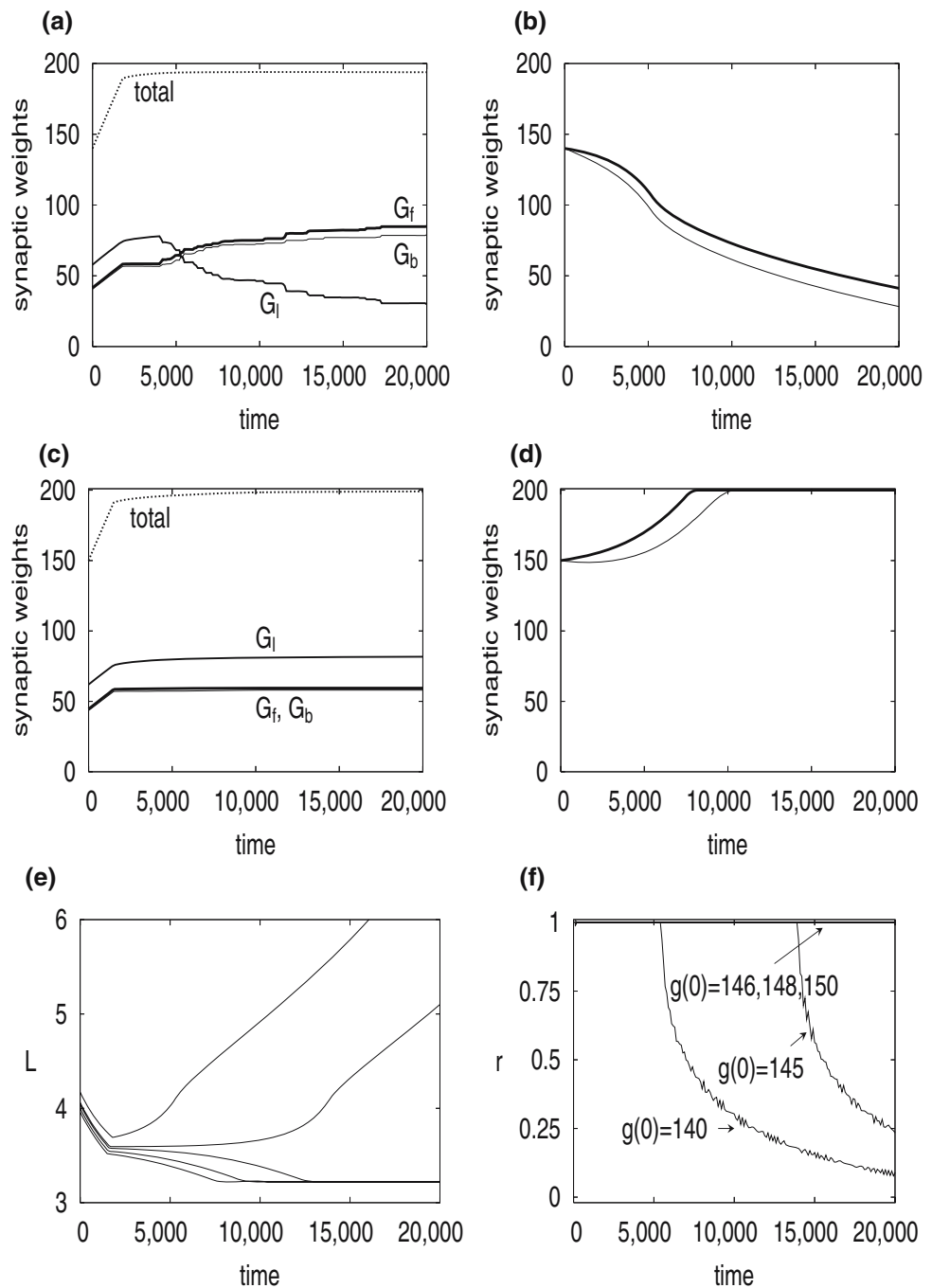
equal to a few milliseconds. The value of  $g_{c-stdp}$  hardly changes with this synaptic delay (results not shown).

To examine the effect of heterogeneity in oscillators, we pick the intrinsic frequency of each oscillator from the gaussian distribution with mean  $\omega = 8.1$  and standard deviation 0.1. Time courses of  $r$  are shown in Fig. 5(h). We estimate  $1.2 < g_{c-stdp} < 1.5$ , implying the robustness of our results against heterogeneity. We remark that  $r$  converges to a positive level when  $g < g_{c-stdp}$ . This is because, even if the oscillators disconnect from the pacemaker, some oscillators form feedforward networks of small size in which fast oscillators entrain and speed up slow oscillators. If the heterogeneity is even larger so that some oscillators are as fast as the pacemaker, frequency synchrony seeding from the pacemaker would be difficult because the pacemaker and fast oscillators compete in entraining slow oscillators.

#### 4.4 Symmetric learning window

Now we examine symmetric STDP. We set  $g_{max} = 200 > g_c \cong 100.7$  so that frequency synchrony with

**Fig. 7** Results for 100 randomly coupled oscillators subject to symmetric STDP. Evolution of the synaptic weights are shown for  $g(0) = 140$  (**a, b**) and  $g(0) = 150$  (**c, d**). See the caption of Fig. 5 for legends. In (**c**),  $G_f$  (thick solid line) and  $G_b$  (thin solid line) overlap almost completely. Time courses of (**e**)  $L$  and (**f**)  $r$  are compared for  $g(0) = 140, 145, 146, 148,$  and  $150$ . In (**e**), lower lines correspond to larger  $g(0)$ . (**g**) Final network structure for  $g(0) = 150$



small phase lags is achieved if  $g_{ji} = g_{max}$  for all  $(j, i) \in E$ . For the network same as that used in Section 4.3, evolution of synaptic weights are summarized in Figs. 7(a, b) and (c, d) for  $g(0) = 140$  and  $g(0) = 150$ , respectively. Because the oscillators share an identical natural frequency, the phases are fairly close among them even with weak coupling. The synapses among these oscillators are potentiated. Accordingly, for both values of  $g(0)$ , the average synaptic weight initially increases (dotted lines in Fig. 7(a, c)). Note that the for-

ward weights ( $G_f$ , thick solid lines in Fig. 7(a, c)) and the backward weights ( $G_b$ , thin solid lines in Fig. 7(a, c)) are equally potentiated. Accordingly, the distance between the oscillators is initially shortened to result in a decrease in  $L$  (Fig. 7(e),  $t \leq 2000$ ).

When  $g(0) = 140$ , the average synaptic weight stops increasing at a value slightly smaller than  $g_{max} = 200$  (dotted line in Fig. 7(a)). This is because the synapses linking the pacemaker to the oscillators have not been potentiated. Actually,  $G_f^0$  (thick line in Fig. 7(b)) and

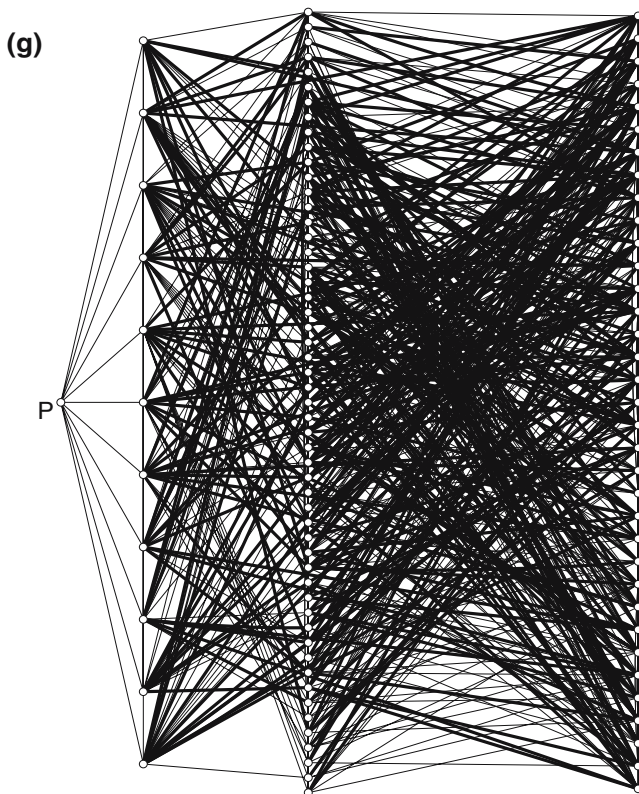


Fig. 7 continued

$G_b^0$  (thin line in Fig. 7(b)) decrease to eventually decouple the oscillators from the pacemaker. Consequently,  $L$  diverges (uppermost line in Fig. 7(e)), and frequency synchrony is eventually lost (Fig. 7(f)).

When  $g(0) = 150$ ,  $G_f^0$  (thick line in Fig. 7(d)) and  $G_b^0$  (thin line in Fig. 7(d)) as well as  $G_f$  (thick solid line in Fig. 7(c)) and  $G_b$  (thin solid line in Fig. 7(c)) increase. Consequently,  $L$  continues to decrease to reach the minimum possible value for which  $g_{ji} = g_{max}$  is achieved for most synapses (lowermost line in Fig. 7(e)). The synchrony measure  $r$  stays near unity throughout (Fig. 7(f)). In fact, approximate phase synchrony as well as frequency synchrony has been realized quickly. The synchrony arises not owing to STDP but to sufficiently strong initial coupling.

Based on Figs. 7(e) and (f), which show time courses of  $L$  and  $r$  for several values of  $g(0)$ , we estimate  $145 < g_{c-stdp} < 146$ . This value of  $g_{c-stdp}$  is much larger than the case of asymmetric STDP and comparable to  $g_c \approx 100.7$ , that is, the threshold for frozen synapses.

The fact that symmetric STDP does not promote frequency synchrony manifests the importance of the feedforwardness of networks. In general, forward synapses promote frequency synchrony, whereas backward synapses hamper it (Kori and Mikhailov 2004). Symmetric STDP does not independently control for-

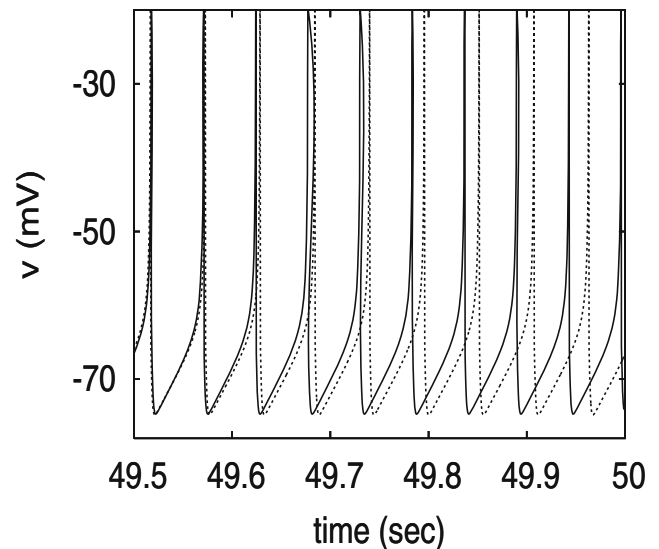


Fig. 8 Sample traces of  $v_0$  (solid line) and  $v_1$  (dashed line) when the spiking neurons are uncoupled

ward synaptic weights and backward synaptic weights. Consequently, it cannot get rid of backward synapses without sacrificing forward synapses. Final network structure is shown for  $g(0) = 150$  in Fig. 7(g). In contrast to the case of asymmetric STDP (Fig. 5(g)), many backward synapses (thick lines) remain. Under symmetric STDP, frequency synchrony is due to strong mutual interaction but not to formation of a feedforward network.

## 5 Networks of pulse-coupled spiking neurons

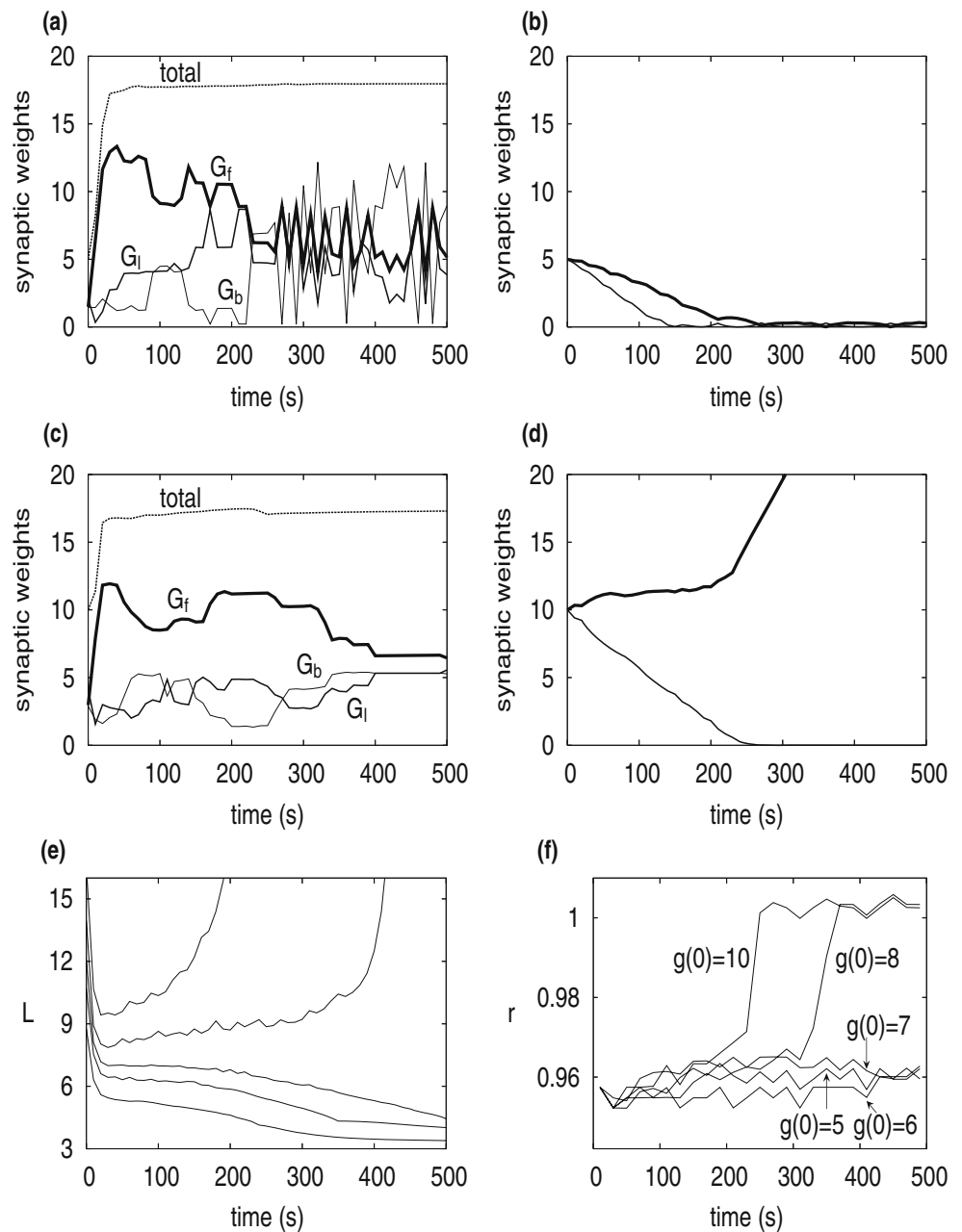
To inspect whether the results obtained for coupled phase oscillators qualitatively apply to more general neuron models, we numerically simulate pulse-coupled spiking neurons under STDP. We adopt a two-dimensional neuron model (Izhikevich 2003; Izhikevich et al. 2004). The subthreshold dynamics of the  $i$ th neuron are described by

$$\dot{v}_i = 0.04v_i^2 + 5v_i + 140 - u_i - I_{syn,i} - I_{ext,i}, \quad (36)$$

$$\dot{u}_i = a(bv_i - u_i), \quad (37)$$

where  $v_i$  is the membrane potential (mV),  $u_i$  denotes the recovery variable that evolves slowly relative to  $v_i$ , and the time unit is millisecond. The spiking mechanism is implemented by resetting the dynamical variables to  $(v_i, u_i) = (c, d)$  as soon as  $v_i$  exceeds 30 mV. We set  $a = 0.02$ ,  $b = 0.2$ ,  $c = -65$ , and  $d = 8$ , which are standard parameter values for modeling pyramidal neurons (Izhikevich 2003; Izhikevich et al. 2004).

**Fig. 9** Results for 100 randomly coupled spiking neurons subject to asymmetric STDP. Evolution of the synaptic weights are shown for (a, b)  $g(0) = 5$  and (c, d)  $g(0) = 10$ . See the caption of Fig. 5 for legends. Time courses of (e)  $L$  and (f)  $r$  are compared for  $g(0) = 5, 6, 7, 8,$  and  $10$ . In (e), lower lines correspond to larger  $g(0)$



The input  $I_{ext,i}$  and  $I_{syn,i}$  are the external bias input and the synaptic input, respectively. We set  $I_{ext,0} = 8.4$  and  $I_{ext,i} = 8$  ( $1 \leq i \leq n - 1$ ). The inherent firing rate of the pacemaker (= 18.8 Hz) is about 5 % higher than that of the oscillators (= 17.9 Hz). In Fig. 8, example traces of the membrane potentials of the pacemaker (solid line) and that of an oscillator (dashed line) are shown.

The synaptic input  $I_{syn,i}$  is composed of superposition of incident spikes from the neurons presynaptic to the  $i$ th neuron. A presynaptic spike of the  $j$ th neuron ( $(j, i) \in E$ ) is assumed to change the postsynaptic

membrane potential according to the time course given by the alpha function:

$$g_{ji}s(t) = g_{ji}\alpha^2te^{-\alpha t}, \quad t \geq 0, \tag{38}$$

where  $t = 0$  corresponds to the spike time. We set  $\alpha = 1$ , so that the unit synaptic input  $s(t)$  peaks at  $t = 1/\alpha = 1$  ms and then decays slowly. We set  $A^+ = 0.09$ ,  $A^- = 0.1$ , and  $\tau = 10$  ms.

The random network with  $n = 100$  used in the following simulations are the same as that used in Section 4. We set the initial synaptic weight  $g_{ji} = g(0)$  for

all the synapses. The initial values of  $v_i$  and  $u_i$  are independently chosen according to the uniform distributions on  $[-75, -50]$  and  $[-8, -6]$ , respectively. Under these conditions, we track time courses of  $G_f$ ,  $G_b$ ,  $G_i$ ,  $G_f^0$ ,  $G_b^0$ ,  $L$  defined in Section 4.2, and  $r = r([t_1, t_2])$  redefined based on spike counts:

$$r = \frac{\frac{1}{n-1} \sum_{i=1}^{n-1} (\text{number of spikes from the } i\text{th neuron})}{(\text{number of spikes from the pacemaker})}. \quad (39)$$

Frequency synchrony yields  $r \cong 1$ . If the pacemaker and the oscillators fire independently,  $r$  is the ratio of the single-neuron firing rate to the pacemaker firing rate. We set  $t_2 - t_1 = 10000$  ms.

With these parameter values, we first determined  $g_c$  without STDP. We numerically obtained  $g_c \cong 1.6$  for the network of one pacemaker and one oscillator, and  $g_c \cong 38$  for the random network. In the following simulations with asymmetric STDP, we set  $g_{max} = 35 < g_c$  so that uniform increases in  $g_{ji}$  do not cause synchronization. Frequency synchrony requires feedforward network structure.

For homogeneous initial synaptic weights  $g(0) = 5$  and  $g(0) = 10$ , evolution of synaptic weights via asymmetric STDP is shown in Fig. 9(a, b) and (c, d), respectively. For  $g(0) = 5$ ,  $G_f$  (thick solid line in Fig. 9(a)) and  $G_f^0$  (thick line in Fig. 9(b)) do not grow during the course of plasticity, similar to Figs. 5(a, b). The oscillators disconnect from the pacemaker, and frequency synchrony is not realized (Fig. 9(f)). For  $g(0) = 10$ , the forward connection from the pacemaker to the set of oscillators is established (thick line in Fig. 9(d)), and backward connection is gradually removed (thin line in Fig. 9(d)), similar to Figs. 5(c, d). As a result, frequency synchrony is reached (Fig. 9f). Based on Figs. 9(e) and 9(f), which respectively show  $L$  and  $r$  for different  $g(0)$ , we estimate  $g_{c-stdp} \cong 7$ , which is much smaller than  $g_c \cong 38$ . Note that  $g(0) = 7$  is a marginal case, which yields a long transient before frequency synchrony is reached. Frequency synchrony is not induced with, for example,  $g(0) = 10 < g_c$  if synapses are frozen. These numerical simulations confirm that the results derived in the previous sections apply to networks of pulse-coupled spiking neurons.

## 6 Discussion

We have shown that asymmetric STDP greatly reduces the threshold for frequency synchronization of neural networks with a pacemaker. This reduction is

efficient particularly when LTP and LTD are nearly balanced, as assumed for stabilization of synaptic weights in previous literature (Kempster et al. 1999; Song et al. 2000; Song and Abbott 2001; van Rossum et al. 2000). Our analytical results for two-oscillator networks provide theoretical understanding of STDP-induced synchrony of two-body networks with real neurons (Nowotny et al. 2003) and with Hodgkin–Huxley neurons (Zhigulin et al. 2003). Our numerical results for large networks extend earlier numerical simulations (Zhigulin and Rabinovich 2004) and provide mechanisms of synchrony.

More microscopically, we have shown that STDP guides formation of feedforward networks originating from the pacemaker (Fig. 5(g)). By eliminating backward connection, frequency synchrony is promoted in terms of required synaptic weights. Networks self-organize by asymmetric STDP so that upstream neurons entrain downstream neurons. Even though engineered learning algorithms can promote formation of feedforward networks (Kori and Mikhailov 2006), asymmetric STDP naturally achieves this goal. Facilitation of frequency synchrony does not occur for symmetric STDP, which cannot suppress backward synapses without sacrificing forward synapses.

In recurrent networks, synaptic delay may destabilize otherwise stable synchrony, leading to oscillatory or chaotic population dynamics (e.g. Gerstner and van Hemmen 1993; Gerstner 2000; Timme et al. 2002). However, our numerical simulations suggest that this is not the case in our system, which can be explained as follows. In the phase oscillator model, the effect of delay can be replaced in a good approximation by the phase shift in the coupling function (Kori and Kuramoto 2001; Kori 2003). Dynamics of the oscillator system under consideration do not change qualitatively for a large class of the coupling function (Kori and Mikhailov 2006), which effectively includes the case of synaptic delay. Although a synaptic delay enlarges the phase difference between connected neurons, the oscillator dynamics in our model are thus robust against delay. Another possible complication is that synaptic delay may change synaptic evolution because it could interact with the learning window. However, since the delay simply increases the phase difference between connected neurons, the causality of spike timing does not change even with delay, as corroborated by our numerical experiments.

In terms of network structure, the feedforward structure is distinct from pruning of synapses in a predefined unidirectional network with many presynaptic neurons projecting to a single postsynaptic neuron (Kempster et al. 1999; Song et al. 2000; Song and Abbott

2001; van Rossum et al. 2000). It also differs from multipartite networks each part of which forms a cluster of synchronously firing neurons (Horn et al. 2000; Levy et al. 2001). In a sense, feedforward structure and hierarchy are straightforward consequences of asymmetric STDP (Song and Abbott 2001), which opts for causality. We stress that feedforward structure is naturally organized when a network has a distinct pacemaker. The idea of growing feedforward structure by unsupervised learning dates back to pioneering work by Bienenstock (1991, 1995), which employed Hebbian plasticity. We have analyzed the network formation in detail under asymmetric STDP. In real neural networks, there may be multiple pacemakers as well as a huge number of follower neurons. It is straightforward to extend our results to the case in which a collection of neurons in a network serves as a pacemaker. Pacemaker neurons are relevant to, for example, regulation of respiration, internal clock, and Parkinsonian diseases (see Section 1 for references). In these brain regions, pacemaker neurons may recruit downstream neurons for frequency synchrony in order to, for example, amplify rhythmic activity.

Formation of feedforward structure could occur even when predetermined pacemakers are absent. In this case, neurons with relatively high natural frequencies may play a role of pacemaker. Backward connection to these fast neurons, which would perturb their periodic firing, can be eventually eliminated by asymmetric STDP. Then, the fast neurons can serve as distinct pacemakers. Regardless of the initial presence of pacemakers, asymmetric STDP creates frequency synchrony, which can be called *feedforward synchrony*. This mechanism of synchrony differs from that of synchrony based on mutual coupling (Kuramoto 1984).

Our results do not suggest that asymmetric STDP promotes phase synchrony, namely, spike synchrony. This is in contrast to the finding that phase synchrony is caused by asymmetric STDP (Karbowski and Ermentrout 2002). In their work, fixed inhibitory coupling as well as excitatory coupling with asymmetric STDP was assumed. Perfectly balanced LTP and LTD, at least as the average, is a key condition for the maintenance of bidirectional connectivity and phase synchrony. By contrast, we assumed that LTD is stronger than LTP. This yields a considerable decrease in the threshold for synchrony. However, this synchrony is frequency synchrony but not spike synchrony.

With symmetric STDP, neurons whose spike times are close are likely to bind together. Then, in addition to frequency synchrony, approximate phase synchrony whose time resolution is specified by the width of the learning window can develop (Seliger et al. 2002). In

some situations, neurons divide into clusters in each of which rough spike synchrony is maintained (Masuda and Aihara 2004). Unlike asymmetric STDP, symmetric STDP does not lessen the threshold for synchrony.

When feedforward frequency synchrony is achieved, neurons at different distances from the pacemaker fire asynchronously. On top of that, phase synchrony can be observed for neurons receiving the common signal. For example, the neurons directly connected to the pacemaker are excited by the common drive from the pacemaker, so that they are synchronized in phase. Likewise, neurons with the same distance from the pacemaker tend to fire simultaneously. Indeed, Fig. 6(b) and its magnification in Fig. 6(c) indicate that clusters of phase-synchronized neurons can be aligned according to the distance from the pacemaker (Kori and Mikhailov 2004). Even though spike time difference between neurons with different distances is usually small, the order of firing is fixed and reproducible. The pacemaker triggers a volley of spikes, which travels down the hierarchy delineated by the distance. This phenomenon is consistent with propagation of synfire volley through feedforward neural networks in the excitable regime (Bienenstock 1995; Diesmann et al. 1999; Reyes 2003; Vogels and Abbott 2005). However, stably embedding synfire volley in recurrent networks is usually difficult (Mehring et al. 2003). It needs, for example, selective enhancement of forward synapses by 10-fold, which corresponds to large evoked EPSPs of 8 mV (Vogels and Abbott 2005). With asymmetric STDP, forward synapses are enhanced. In addition, automatic elimination of backward synapses appreciably lessens the forward synaptic strength (or the size of EPSP) needed for stable synfire volley.

We have shown that the facilitation of frequency synchrony by STDP is robust against some heterogeneity in the inherent firing frequency of the neurons. If synaptic delays or neurons are strongly heterogeneous, we would obtain more complex but reproducible spatiotemporal spike patterns (Izhikevich et al. 2004; Izhikevich 2006; Lengyel et al. 2005).

Oscillatory neurons can model, for example, temporal coding of place cells (Mehta et al. 2002) and hippocampal associative memory (Lengyel et al. 2005). By contrast, many neural circuits operate in the excitable regime, in which neurons are not spontaneously oscillatory. Investigation of the excitable case is warranted for future studies. However, we believe that the conclusion that asymmetric STDP but not symmetric STDP induces feedforward synchrony generalizes to the excitable case, as is consistent with previous numerical work (Song and Abbott 2001; Zhigulin and Rabinovich 2004).

**Acknowledgements** We thank Brent Doiron and Taro Toyozumi for critical reading of the manuscript and Tohru Ikeguchi and Tomoya Suzuki for discussion. Naoki Masuda thanks the Special Postdoctoral Researchers Program of RIKEN. Hiroshi Kori thanks financial support from the Humboldt foundation (Germany) and from 21st Century COE program “Nonlinearity via Singularity” in Department of Mathematics, Hokkaido University.

## References

- Abbott, L. F., & Nelson, S. B. (2000). Synaptic plasticity: Taming the beast. *Nature Neuroscience Supp.*, *3*, 1178–1183.
- Bienenstock, E. (1991). Notes on the growth of a composition machine. In D. Andler, E. Bienenstock, & B. Laks (Eds.), *Proceedings of the First Interdisciplinary Workshop on Compositionality in Cognition and Neural Networks* (pp. 25–43). Abbaye de Royaumont, France.
- Bienenstock, E. (1995). A model of neocortex. *Network: Computation in Neural Systems*, *6*, 179–224.
- Braunstein, L. A., Buldyrev, S. V., Cohen, R., Havlin, S., & Stanley, H. E. (2003). Optimal paths in disordered complex networks. *Physical Review Letters*, *91*, 168701.
- Bell, C. C., Han, V. Z., Sugawara, Y., & Grant, K. (1997). Synaptic plasticity in a cerebellum-like structure depends on temporal order. *Nature*, *387*, 278–281.
- Bi, G., & Poo, M. (1998). Synaptic modifications in cultured hippocampal neurons: dependence on spike timing, synaptic strength, and postsynaptic cell type. *Journal of Neuroscience*, *18*(24), 10464–10472.
- Buzsáki, G., & Draguhn, A. (2004). Neuronal oscillations in cortical networks. *Science*, *304*, 1926–1929.
- Dan, Y., & Poo, M. (1992). Hebbian depression of isolated neuromuscular synapses in vitro. *Science*, *256*, 1570–1573.
- Diesmann, M., Gewaltig, M.-O., & Aertsen, A. (1999). Stable propagation of synchronous spiking in cortical neural networks. *Nature*, *402*, 529–533.
- Froemke, R. C., & Dan, Y. (2002). Spike-timing-dependent synaptic modification induced by natural spike trains. *Nature*, *416*, 433–438.
- Gerstner, W., & van Hemmen, J. L. (1993). Coherence and incoherence in a globally coupled ensemble of pulse-emitting units. *Physical Review Letters*, *71*, 312–315.
- Gerstner, W., Kempter, R., van Hemmen, J. L., & Wagner, H. (1996). A neuronal learning rule for sub-millisecond temporal coding. *Nature*, *383*, 76–78.
- Gerstner, W. (2000). Population dynamics of spiking neurons: Fast transients, asynchronous states, and locking. *Neural Computation*, *12*, 43–89.
- Gerstner, W., & Kistler, W. M. (2002). *Spiking neuron models*. Cambridge: Cambridge University Press.
- Glass, L., & Mackey, M. C. (1988). *From clocks to chaos—The rhythms of life*. Princeton: Princeton University Press.
- Hansel, D., Mato, G., & Meunier, C. (1993). Phase dynamics for weakly coupled Hodgkin–Huxley neurons. *Europhysics Letters*, *23*(5), 367–372.
- Hansel, D., Mato, G., & Meunier, C. (1995). Synchrony in excitatory neural networks. *Neural Computation*, *7*, 307–337.
- Horn, D., Levy, N., Meilijson, I., & Ruppin, E. (2000). Distributed synchrony of spiking neurons in a Hebbian cell assembly. In S. A. Solla, T. K. Leen, & K.-R. Müller (Eds.), *Advances in Neural Information Processing Systems*, (Vols. 25–43, pp. 129–135). Cambridge, MA: MIT.
- Hutcheon, B., & Yarom, Y. (2000). Resonance, oscillation and the intrinsic frequency preferences of neurons. *Trends in Neurosciences*, *23*(5), 216–222.
- Izhikevich, E. M. (2003). Simple model of spiking neurons. *IEEE Transactions on Neural Networks*, *14*(6), 1569–1572.
- Izhikevich, E. M. (2006). Polychronization: Computation with spikes. *Neural Computation*, *18*, 245–282.
- Izhikevich, E. M., Gally, J. A., & Edelman, G.M. (2004). Spike-timing dynamics of neuronal groups. *Cerebral Cortex*, *14*(8), 933–944.
- Jefferys, J. G. R., Traub, R. D., & Whittington, M. A. (1996). Neuronal networks for induced ‘40 Hz’ rhythms. *Trends in Neurosciences*, *19*(5), 202–208.
- Karbowski, J., & Ermentrout, G. B. (2002). Synchrony arising from a balanced synaptic plasticity in a network of heterogeneous neural oscillators. *Physical Review E*, *65*, 031902.
- Kempter, R., Gerstner, W., & van Hemmen, J. L. (1999). Hebbian learning and spiking neurons. *Physical Review E*, *59*, 4498–4514.
- Kori, H. (2003). Slow switching in a population of delayed pulse-coupled oscillators. *Physical Review E*, *68*, 021919.
- Kori, H., & Kuramoto, Y. (2001). Slow switching in globally coupled oscillators: Robustness and occurrence through delayed coupling. *Physical Review E*, *63*, 046214.
- Kori, H., & Mikhailov, A. S. (2004). Entrainment of randomly coupled oscillator networks by a pacemaker. *Physical Review Letters*, *93*, 254101.
- Kori, H., & Mikhailov, A. S. (2006). Strong effects of network architecture in the entrainment of coupled oscillator systems. *Physical Review E*, *74*, 066115.
- Kuramoto, Y. (1984). *Chemical oscillations, waves, and turbulence*. Berlin: Springer.
- Kuramoto, Y. (1991). Collective synchronization of pulse-coupled oscillators and excitable units. *Physica D*, *50*, 15–30.
- Lengyel, M., Kwag, J., Paulsen, O., & Dayan, P. (2005). Matching storage and recall: Hippocampal spike timing-dependent plasticity and phase response curves. *Nature Neuroscience*, *8*, 1677–1683.
- Levy, N., Horn, D., Meilijson, I., & Ruppin, E. (2001). Distributed synchrony in a cell assembly of spiking neurons. *Neural Networks*, *14*, 815–824.
- Markram, H., Lübke, J., Frotscher, M., & Sakmann, B. (1997). Regulation of synaptic efficacy by coincidence of postsynaptic APs and EPSPs. *Science*, *275*, 213–215.
- Masuda, N., Aihara, K. (2004). Self-organizing dual coding based on spike-time-dependent plasticity. *Neural Computation*, *16*, 627–663.
- Mehring, C., Hehl, U., Kubo, M., Diesmann, M., & Aertsen, A. (2003). Activity dynamics and propagation of synchronous spiking in locally connected random networks. *Biological Cybernetics*, *88*, 395–408.
- Mehta, M. R., Lee, A. K., & Wilson, M. A. (2002). Role of experience and oscillations in transforming a rate code into a temporal code. *Nature*, *417*, 741–746.
- Nishiyama, M., Hong, K., Mikoshiba, K., Poo, M., & Kato, K. (2000). Calcium stores regulate the polarity and input specificity of synaptic modification. *Nature*, *408*, 584–588.
- Nowotny, T., Zhigulin, V. P., Selverston, A. I., Abarbanel, H. D. I., & Rabinovich, M. I. (2003). Enhancement of synchrony

- nization in a hybrid neural circuit by spike-timing dependent plasticity. *Journal of Neuroscience*, 23(30), 9776–9785.
- Pikovsky, A., Rosenblum, M., & Kurths, J. (2001). *Synchronization—A universal concept in nonlinear sciences*. Cambridge, UK: Cambridge University Press.
- Plenz, D., & Kitai, S. T. (1999). A basal ganglia pacemaker formed by the subthalamic nucleus and external globus pallidus. *Nature*, 400, 677–682.
- Ramirez, J.-M., Tryba, A. K., & Peña, F. (2004). Pacemaker neurons and neuronal networks: An integrative view. *Current Opinion in Neurobiology*, 14, 665–674.
- Reyes, A. D. (2003). Synchrony-dependent propagation of firing rate in iteratively constructed networks *in vitro*. *Nature Neuroscience*, 6(6), 593–599.
- Ritz, R., & Sejnowski, T. J. (1997). Synchronous oscillatory activity in sensory systems: New vistas on mechanisms. *Current Opinion in Neurobiology*, 7, 536–546.
- Seliger, P., Young, S. C., & Tsimring, L. S. (2002). Plasticity and learning in a network of coupled phase oscillators. *Physical Review E*, 65, 041906.
- Shouval, H. Z., Bear, M. F., & Cooper, L. N. (2002). A unified model of NMDA receptor-dependent bidirectional synaptic plasticity. *Proceedings of the National Academy of Sciences, USA*, 99(16), 10831–10836.
- Singer, W., Gray, & C. M. (1995). Visual feature integration and the temporal correlation hypothesis. *Annual Review of Neuroscience*, 18, 555–586.
- Song, S., & Abbott, L. F. (2001). Cortical development and remapping through spike timing-dependent plasticity. *Neuron*, 32, 339–350.
- Song, S., Miller, K. D., & Abbott, L. F. (2000). Competitive Hebbian learning through spike-timing-dependent synaptic plasticity. *Nature Neuroscience*, 3(9), 919–926.
- Timme, M., Wolf, F., & Geisel, T. (2002). Prevalence of unstable attractors in networks of pulse-coupled oscillators. *Physical Review Letters*, 89, 154105.
- van Rossum, M. C. W., Bi, G. Q., & Turrigiano, G. G. (2000). Stable Hebbian learning from spike timing-dependent plasticity. *Journal of Neuroscience*, 20(23), 8812–8821.
- Vogels, T. P., & Abbott, L. F. (2005). Signal propagation and logic gating in networks of integrate-and-fire neurons. *Journal of Neuroscience*, 25(46), 10786–10795.
- Winfree, A. T. (1980). *The geometry of biological time*. New York: Springer.
- Woodin, M. A., Ganguly, K., & Poo, M. (2003). Coincident pre- and postsynaptic activity modifies GABAergic synapses by postsynaptic changes in Cl<sup>-</sup> transporter activity. *Neuron*, 39, 807–820.
- Zhang, L. I., Tao, H. W., Holt, C. E., Harris, W. A., & Poo, M. (1998). A critical window for cooperation and competition among developing retinotectal synapses. *Nature*, 395, 37–44.
- Zhigulin, V. P., & Rabinovich, M. I. (2004). An important role of spike timing dependent synaptic plasticity in the formation of synchronized neural ensembles. *Neurocomputing*, 58–60, 373–378.
- Zhigulin, V. P., Rabinovich, M. I., Huerta, R., & Abarbanel, H. D. I. (2003). Robustness and enhancement of neural synchronization by activity-dependent coupling. *Physical Review E*, 67, 021901.